International Journal of Pharmaceutics 383 (2010) 70–80

Contents lists available at ScienceDirect

International Journal of Pharmaceutics

journal homepage: www.elsevier.com/locate/ijpharm

# Prediction of drug particle size and content uniformity in low-dose solid dosage forms

Chien-Yueh Huang*, M. Sherry Ku

*Pharmaceutical Development, Wyeth Research, 401 N. Middletown Road, Pearl River, NY 10965, United States*

ARTICLE INFO

*Article history:*
Received 18 June 2009
Received in revised form 3 September 2009
Accepted 4 September 2009
Available online 10 September 2009

*Keywords:*
Content uniformity
Particle size
Low-dose drugs
Monte Carlo
Mixing
Blending
Poisson distribution

ABSTRACT

Drug particle size distribution has a profound impact to the content uniformity in low-dose solid drug products. We derived theoretically the skewness of potency distribution as a function of particle size distribution and target dose. It was demonstrated that both skewness and coefficient of variation diverge simultaneously with inverse square root of the target dose. This scaling relation was observed in recent experiment and was verified by Monte Carlo (MC) simulation, which was employed for the first time to solve for the full potency distribution from a random retrieving model. When tested against the criteria from USP ⟨905⟩ uniformity of dosage units, MC simulation showed a striking anisotropic distribution of the data. This suggests a full-scale consideration of the potency distribution is necessary for evaluating the impacts from particle size distribution and the dose, as compared against the normality assumption used before. A nomograph of the median particle size and the dose that meets a 99% pass rate was constructed for the specification of particle size or the lowest dose limit. Furthermore, we showed quantitatively the lowest dose limit can be drastically reduced if a cut-off size is imposed by removing oversized particles.


## 1. Introduction

Particle size distribution (PSD) of active pharmaceutical ingredient (API) is the most critical quality attribute followed by non-ideal mixing impacting the uniformity of solid dosage forms, in particular for low-dose drugs (Gordon et al., 1990; Zheng, 2009). A smaller API particle size can enhance the statistics of an even distribution of API among the dosage units and increase the dissolution due to a larger specific surface area. However, it may hinder the processibility with agglomeration (Orr and Shotton, 1973; Egermann et al., 1985; Cartilier and Moes, 1989) and result in segregation and poor blending uniformity. This is because of mismatch in particle size and shape (Rhodes, 2008; Jullien and Meakin, 1990), surface energy, cohesiveness, and adhesive interaction (Israelachvili, 1995; Buckton, 1995; Podczeck, 1998), electrostatics (Podczeck, 1998; Byron et al., 1997; Lachiver et al., 2006), etc.—just to name a few. A larger size may improve the processibility but compromise the uniformity: the presence of a large API particle in a dosage unit (capsule or tablet) renders it over-potent but leaves the rest units under-potent which likely results in the observation of an under-potent batch based on finite sampling. How to balance the demands on uniformity, processibility, and dissolution performance by specifying an appropriate API particle size distribution is a constant and profound challenge in pharmaceutical development. Particularly, such a decision has to be made in an early stage based on data generated by a limited amount of API solid. A reliable expert system would be invaluable for specifying an appropriate particle size based on the physical and chemical nature of the pharmaceutical ingredients.

Theoretical treatments for the relation between API particle size and drug product content uniformity (CU) (Train, 1960; Hersey, 1967; Johnson, 1972; Yalkowsky and Bolton, 1990; Rohrs et al., 2006) can be tracked back to random mixing theory for powders (Lacey, 1943; Stange, 1954; Poole et al., 1964). Johnson (1972, 1974, 1975) applied a random retrieving model to derive the dependence of drug content variation on API particle size distribution. The ensemble of dosage units was constructed via random retrieving of ideally mixed API particles that follows Poisson statistics. The applicability of the model relies on the good faith of ideal mixing, which can be interpreted as the lack of spatial correlation for API particles beyond the length scale of the dosage unit. In reality, this may be achieved through various techniques such as granulations. The applicability is also limited by the occurrence of significant particle size reduction during the mixing and other processing steps. The particle size distribution used for the model should be the final size distribution before tabletting or capsulation. For cohesive powders that form strong agglomerates (Orr and Shotton, 1973), each agglomerate entity should be regarded as a single large particle. Only under the circumstance that the API particles do not experience significant size reduction or form unbreakable agglomerates,

* Corresponding author. Tel.: +1 845 602 3048; fax: +1 845 602 4936.
*E-mail address:* huangm4@wyeth.com (C.-Y. Huang).

0378-5173/$ – see front matter © 2009 Elsevier B.V. All rights reserved.
doi:10.1016/j.ijpharm.2009.09.009

the initial API particle size distribution can be used as the input to the model. Using similar assumptions but a different analytical approach, Yalkowsky and Bolton (1990) derived the content variation that is mathematically equivalent to Johnson's. Furthermore, they gave the equation for API with a log-normal particle size distribution and the limit against the USP Content Uniformity test. The equivalency of Johnson's and Yalkowsky's results was confirmed later by Rohrs et al. (2006), who also showed a nomograph of mean particle size and the lowest dose limit for passing USP28/NF23 CU criteria. The equivalency is not surprising since the target dose and the particle size distribution are de-coupled in these models.

The most important result of the above theoretical studies is the coefficient of variation $C_v$ of the drug potency distribution. Based on the predicted $C_v$, a normal potency distribution is assumed and the confidence of passing the CU criteria can be calculated. Note that there is no any theoretical ground that a drug potency distribution must be normal and the skewness (skewness factor, $\alpha_3$) must go to zero. Yalkowsky and Bolton (1990) warned that the potency distribution is not normal if the standard deviation of the API particle size distribution is large. In fact, many experiments showed that the potency distributions were highly skewed. Orr and Shotton (1973) and Orr and Sallam (1978) reported the observation of positive skewness in potency distribution with highly diluted cohesive API powders. They attributed the positive skewness to the agglomerates of the cohesive powders. Sallam and Orr (1985, 1986) proposed a critical API particle size, above which a good mixing can be achieved and that both $C_v$ and $\alpha_3$ increase with the mean particle size. When below the critical size, the API particles are cohesive and form large agglomerates leading to the observation of increasing $C_v$ and $\alpha_3$ with decreasing API particle size. In addition to the particle size distribution, the target dose also affects the skewness. Rohrs et al. (2006) recently reported that under a given particle size distribution, the skewness increases anomalously with decreasing target dose. Reducing the target dose not only results in an increase of $C_v$ of the potency distribution but also leads to a stronger deviation from normality. Therefore, the full spectrum of potency distribution becomes necessary for the study of the content uniformity in low-dose cases. Unfortunately, to date no full solution to the random retrieving theory is available. The only published simulation to construct the potency distribution was reported by Zhang and Johnson (1997) and Johnson (2009) based on even filling of API particles from different bins (sizes) into dosage units. In their model, the variability of each dosage unit is one API particle per bin in contrast to the random retrieving theory, which allows all accessible combinations of API particles from different bins drawn into a dosage unit. Furthermore, Zhang and Johnson's simulation algorithm is deterministic and carries correlation artifacts into statistics. More details will be discussed in Theory.

In this work we applied random retrieving theory to derive the skewness from the third central moment of the potency distribution. We found that the potency distribution will skew toward under-potency while both skewness and coefficient of variation diverge anomalously as the target dose approaches zero. The anomaly, consistent with the observation from experiments, signals the breakdown of the normality assumption used in previous theoretical treatments for low-dose content uniformity. We then applied Monte Carlo method to solve the full potency distribution of the random retrieving theory for the first time. When tested against the criteria from USP ⟨905⟩ uniformity of dosage units, the Monte Carlo simulation showed a striking anisotropic distribution of the data. This observation denotes a tendency that a skewed potency distribution increases the chance of falsely passing the USP criteria which are based on a 95% chance of potency values within the 85–115% label claim assuming a normal potency distribution. Monte Carlo simulation was then employed to construct a large number of CU tests according to USP ⟨905⟩. The pass rate can be calculated according to a given target dose and API particle size distribution. To facilitate a systematic comparison and the application for particle size specification, a nomograph of the median particle size and the dose limit that meets a 99% pass rate was constructed for various $d_{90}/d_{50}$ ratios. We examined special cases when a cut-off limit of oversized particles was imposed and found the passing boundaries on the nomograph changed drastically. This observation indicates that the safety margin to meet the regulatory criteria can increase significantly, or alternatively, the lowest dose limit can be extended to a much smaller value simply by removing oversized particles.

We arranged this article in the following order: the skewness of the potency distribution was derived first followed by the introduction of the Monte Carlo simulation and the computational algorithm. The physical origin of the skewness in the potency distribution was discussed as well as the under-potent batch mean. The nomographs of the lowest dose limit under various geometric standard deviations and cut-off sizes were given followed by the discussion of their applications.

## 2. Theory

### 2.1. Skewness of potency distribution based on a random retrieving theory

The skewness $\alpha_3$ and coefficient of variation $C_v$ derived from a random retrieving theory where the number of API particles in a dosage unit follows a Poisson distribution can be written as

$$\alpha_3 = \frac{\langle w\rangle^{1/2}\langle w^3\rangle}{D^{1/2}\langle w^2\rangle^{3/2}}, \tag{1}$$

$$C_v = \frac{\langle w^2\rangle^{1/2}}{D^{1/2}\langle w\rangle^{1/2}}. \tag{2}$$

Here $D$ is the target dose and $w$ is the equivalent API weight distribution converted from the number frequency-size distribution of the API particles. Detailed derivations are in Appendix A. Several features can be immediately drawn from the equations above. Firstly, the target dose is de-coupled from particle size distribution, which affects the potency fluctuations via various moments of the corresponding weight distribution.

Secondly, both $\alpha_3$ and $C_v$ are proportional to the inverse square root of the target dose. As the target dose approaches zero, $\alpha_3$ and $C_v$ blow up simultaneously. The anomalous increases of $\alpha_3$ and $C_v$ and the scaling relation with low dose have been observed in experiment. Fig. 1(a) and (b) show the re-construction of experiment data by Rohrs et al. (2006) where the percentage coefficient of variation and the skewness are plotted on a log–log scale against the target dose. It is found that in both figures, the data points follow closely the dashed lines which show a slope of $-1/2$ according to the scaling relation from Eqs. (1) and (2). The observed scaling relation supports the legitimacy of the random retrieving theory and the employment of Poisson distribution.

Thirdly, $\alpha_3$ is always positive due to the skewed nature of Poisson distribution and that the number of particles cannot be negative. In experiment, small negative skewness was observed sometimes when the target dose was large or the mean particle size was small (Sallam and Orr, 1985, 1986; Rohrs et al., 2006). This could be due to the variability from finite number of sampling since in either case the theoretical skewness approaches zero. Fourthly, Eq. (1) shows a stronger dependence on the variance of particle size distribution than Eq. (2). Consequently, $\alpha_3$ is more susceptible to low target dose than $C_v$ when the particle size distribution is wide. This notion is immensely critical: as the target dose decreases, the expected potency distribution will quickly deviate from a normal

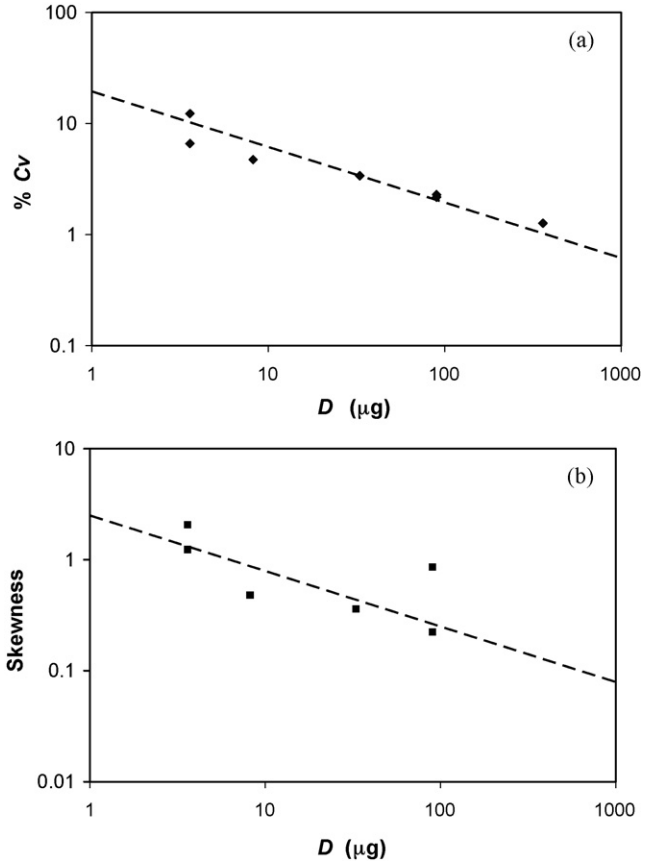


**Fig. 1.** Re-construction of (a) the percentage coefficient of variation and (b) the skewness versus the target dose on a log–log scale from the experiment results by Rohrs et al. (2006). The dashed lines show a slope of −1/2, the scaling relation from Eqs. (1) and (2).

distribution before $C_v$ becomes significantly large. Therefore, the normality assumption breaks down at adequately low target dose. Neglecting this fact could lead to a potential serious problem of over-potent units from the long tail of a positively skewed potency distribution.

To further elucidate the origin of the skewness, Eq. (1) can be written in a discrete form following the notations used in Johnson's paper (Johnson, 1972):

$$\alpha_3 = \sqrt{\frac{\pi\rho}{6D}} \frac{\sum_{i=1}^{N} f_i d_i^6}{\left(\sum_{i=1}^{N} f_i d_i^3\right)^{3/2}}, \tag{3}$$

where $\rho$ is the true density of the API and $f_i$ is the volume faction of API particles from a bin with a volume-equivalent diameter, $d_i$. The fluctuation of number of particles retrieved from the $i$th bin has a simple scaling relation:

$$\frac{\delta n_i}{\langle n_i \rangle} \sim \frac{\sqrt{Var(n_i)}}{\langle n_i \rangle} \sim \left(\frac{D}{\rho} f_i\right)^{-1/2} {d_i}^{3/2}.$$

This relation explains that the augment of the fluctuation field from large particles upon the reduction of dose drives the potency distribution skewed positively. Finally, for the case of a log-normal particle size distribution, Eq. (1) becomes

$$\alpha_3 = \sqrt{\frac{\pi\rho}{6D}} d_m^{3/2} (1 + C^2)^{15}, \tag{4}$$

where $c$ is the arithmetic (number-average) coefficient of variation and $d_m$ is the arithmetic mean diameter of the particle size distribution. Again, Eq. (4) shows a greater susceptibility to the variance of the particle distribution than the coefficient of variation (Eq. (A17) in Appendix A).

### 2.2. Monte Carlo simulation

In this study, Monte Carlo simulation is used to solve the full solution to the random retrieving theory and to simulate content uniformity tests according to USP ⟨905⟩. Monte Carlo simulation finds a wide application in sciences and engineering (Rubinstein and Kroese, 2008; Bonate, 2001; Armitage et al., 2001) where the evolution and properties of a complex dynamic system with a large number of degrees of freedom can be tracked. The algorithm used here is a simple rejection method to construct random events that follow a Poisson probability. Technically, this can be achieved via generating first a deviate of uniform distribution followed by random shooting to obtain a random deviate falling inside a Poisson distribution (Press et al., 2007).

To construct a large ensemble of dosage units, the drug particles are first partitioned into $\mathcal{N}$ bins according to their sizes; each bin has a representative particle diameter. Here, $\mathcal{N} = 300$ is used in all computations. The Poisson probability for a random variable $n_i$ equal to $x$ is expressed as

$$P(x) = \frac{\langle n_i \rangle^x e^{-\langle n_i \rangle}}{x!}, \tag{5a}$$

where $\langle n_i \rangle$ is the average number of particles drawn from the $i$th bin and is determined by

$$\langle n_i \rangle = \frac{6}{\pi\rho} f_i \left(\frac{D^{1/3}}{d_i}\right)^3. \tag{5b}$$

This way, the potency distribution can be constructed by repeatedly generating many dosage units, say an ensemble of 10 million tablets, via a random process of selecting the variables followed by multiplication of the corresponding mass, and summation.

The potency strength distribution is a linear combination of fluctuation from multiple independent bins, or equivalently, modes. The fluctuation of each mode is determined solely by the parameter $\langle n_i \rangle$. If the particle size of every bin is scaled up by a factor of $t$ times (i.e. the entire distribution curve is shifted rightwards by $\ln t$) and the target dose is scaled up by a factor of $t^3$ times, $\langle n_i \rangle$ and, thus, the entire set of parameters remain the same. Consequently, the potency distribution of the scaled up system must be identical to the original potency distribution. Moving along any line with a slope of 1/3 on the logarithmic $d_{50}$–$D$ plot represents the loci of identical potency distribution. This is valid as long as the conformation of the particle size distribution curve remains unchanged during the scaling up, i.e. only a horizontal shift is involved on a semi-log distribution plot. The conclusion is universal for any original particle size distribution. If the conformation is changed such as the intervention by screening off oversized particles (size cut-off), the parameters controlling the multivariate fluctuation will change accordingly. Consequently, the power-law relation for identical potency distribution breaks down. Using this power-law relation would allow one to experimentally verify the random retrieving model with larger API particle sizes and higher doses to circumvent blending heterogeneity caused by fine particles.

Previously, Zhang and Johnson (1997) and Johnson (2009) used computer simulation to study the effect of drug particle size on the content uniformity of low-dose solid dosage forms. Their consideration is based on even filling of API particles from each bin into every dosage unit. Due to the discrete nature of the particles, the average particle number from each bin is divided into an integer part and a remainder, which will rollover during the filling process and appear as an extra particle in every several units i.e. when the accumulated remainder exceeds one. Therefore, all dose units

**Table 1**
Criteria for USP ⟨905⟩ Content Uniformity.

*(A) General formula*

$AV = |M - \bar{X}| + ks, \quad \bar{X} = \frac{1}{n}\sum_{j=1}^{n} x_j, \quad s = \sqrt{\frac{\sum_{j=1}^{n}(x_j - \bar{X})^2}{n-1}}$

*(B) Reference value M*

| | | | | | |
|---|---|---|---|---|---|
| $T \le 101.5$ | $\bar{X} > 101.5$ | $M = 101.5$ | $T > 101.5$ | $\bar{X} > T$ | $M = T$ |
| | $\bar{X} < 98.5$ | $M = 98.5$ | | $\bar{X} < 98.5$ | $M = 98.5$ |
| | $98.5 \le \bar{X} \le 101.5$ | $M = \bar{X}$ | | $98.5 \le \bar{X} \le T$ | $M = \bar{X}$ |

*(C) Acceptance criteria*

| Stage 1 ($n = 10$, $k = 2.4$) | | Stage 2 ($n = 30$, $k = 2$) |
|---|---|---|
| $AV \le L_1$ | $AV \le L_1$ | |
| | $x_{max} \le (1 + L_2 \times 0.01)M$ | |
| | $x_{min} \ge (1 - L_2 \times 0.01)M$ | |

*(D) Notation*

$AV$: Acceptance value; $\bar{X}$: mean; $s$: sample standard deviation
$x_{min}$: minimal individual value; $x_{max}$: maximal individual value
$T$: target content per dosage unit, expressed as the percentage of the label claim: $T$ = D/LC 100%
LC: label claim
$L_1 = 15$ and $L_2 = 25$ unless otherwise specified in the individual monograph

have the same minimal dose strength that corresponds to the integer part from each bin. The variability of the dose strength from one unit to another depends on the combination of the appearance of the extra one particle from each bin. The combination is calculated by a deterministic algorithm that depends on the initial condition. The combination has an upper bound for the maximal strength as the extra one particle from each bin appears simultaneously.

Comparing the Monte Carlo (MC) method and the method by Zhang and Johnson (Z–J), both methods can handle any particle size distribution by partitioning the API particles into different bins according to the sizes. Both methods use the set of average number of particles from each bin as the only set of parameters for simulation. However, the assumptions for the statistical basis and the computation algorithms used in these two models are very different. The differences are explained as follows. Firstly, the MC method creates an ensemble of dosage units representing overlapping of numerous batches of drug products that have been prepared independently to the best extent of mixing and the formation of the dosage units. In fact, any physical dosage unit from manufacturing can find a corresponding configuration in the $\mathcal{N}$-dimension manifold sampled by the MC model. The assumption used in the Z–J method asserts that every particle bin must contribute the same minimum number of particles to every dosage unit; this assumption is not realistic to any known process in practice. Compared to the entire volume of the manifold sampled by the MC method, the accessible states in Z–J method are restricted to the vertices of a cube with unity length in the $\mathcal{N}$-dimension space. The tremendous reduction of entropy in Z–J method imposes a very heavy strain upon the justification of its assumption and does not reflect the random nature of powder mixing.

Secondly, the construction of dosage units in MC method is a random process while in Z–J method it is deterministic. The employment of random process is extremely important (Huang and Muthukumar, 1997; Mamaluy and Huang, 2004) to avoid correlation artifacts in order to obtain a meaningful statistical outcome. The deterministic algorithm used in Z–J method can easily introduce invalid correlation that has no physical ground. For instance, in an example illustrated by Johnson (Fig. 3.1 in Johnson, 2009) that in every 20 dosage units, a particle from a bin, say A, appearing once in every 10 units will *always* appear together with another particle from a different bin, say B, that appears once in every 4 units. However, if the initial condition changes to A particles appearing only in the unit number 1, 11, 21, etc. and B particles appearing in the unit number 4, 8, 12, etc., A and B particles will *never* meet in the same dosage unit. In either case, a correlation artifact is built between the two types of particles and the result depends on the initial condition. The MC method does not include any such artifact or any dependence on the initial condition. Thirdly, the upper bound in Z–J method increases with the number of bins used in the model and the potency profile changes with it as well. One soon falls into a tedious argument on the selection of the system that could not converge to a definite result. The MC method can avoid such a hurdle and show no dependence on the selection of the number of bins once it reaches an adequate resolution.

### 2.3. USP ⟨905⟩ uniformity of dosage units

The new criteria from USP ⟨905⟩ Uniformity of Dosages Units (USP31-NF29, 2009) harmonized with European Pharmacopoeia 2.9.40. Uniformity of dosage units (European Pharmacopoeia, 2008) are based on a two-stage process using acceptance values ($AV$). For content uniformity, 10 dosage units are examined first to obtain the Stage-1 $AV$. If the $AV$ exceeds the criterion, the first test fails and the process will enter Stage 2 by examining additional 20 units. If the Stage-2 $AV$ and the extreme of the 30 units are compliant with the criteria, the test passes. Details of the formula and passing criteria are depicted in Table 1. Note that the new guideline considers simultaneously the interplays of the potency mean ($\bar{X}$), the sample standard deviation ($s$), and the ratio of the target dose to the label claim. In order to pass the Stage 1, the mean and standard deviation of the samples must fall, schematically, inside a trapezoidal area defined by the criteria. It is, however, complicated to predict the conditions based a given confidence. Bergum and Li (2007) and Cholayudth (2008) applied probability analysis to evaluate the pass rates based on the assumption of normal distributions. Their derivations involved various approximations and required numerical integrations. Moving beyond the assumption of normality, the analytical tractability is dim.

### 2.4. Numerical algorithm

To facilitate a systematic investigation on the interplays of the particle size, standard deviation, and the lowest dose limit, we hereafter focus only on log-normal particle size distribution that takes the following form in our analysis:

$$f(d) = \frac{1}{\sqrt{2\pi}\ln\sigma_g}\exp\left(-\frac{(\ln d - \ln d_{50})^2}{2(\ln\sigma_g)^2}\right). \quad (6)$$

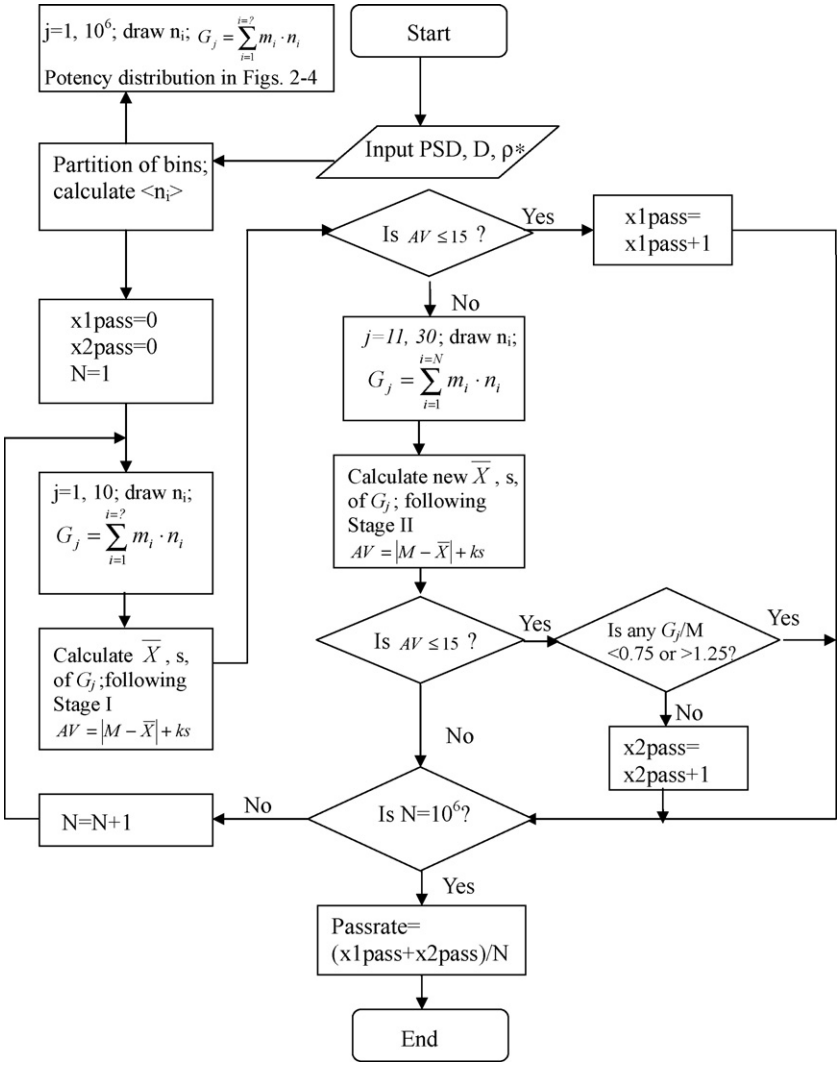


**Fig. 2.** The flowchart of the simulation algorithm. In addition to the variables defined in Appendix A and Table 1, x1pass and x2pass are the counts for passing Stages 1 and 2, respectively; $N$ is the count for CU tests. $n_i$ is the particle number randomly drawn from the $i$th bin and $m_i$ is the equivalent spherical volume of the corresponding particle. The Passrate is the sum of x1pass and x2pass divided by $N$.

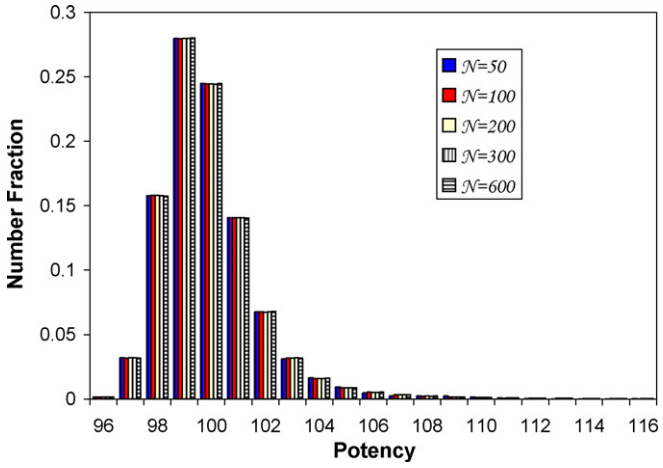


**Fig. 3.** Effect of the number of bins $\mathcal{N}$ on the potency distribution calculated from log-normal API size distribution with $d_{50}$ = 10 μm, $\sigma_g$ = 3.5, and $D/\rho$ = 0.462 mg. A larger $\mathcal{N}$ denotes a finer partition that mimics a continuous distribution on the cost of longer computation time. The figure shows no significant difference among the $\mathcal{N}$s tested; an $\mathcal{N}$ = 300 is selected for all computations hereafter.

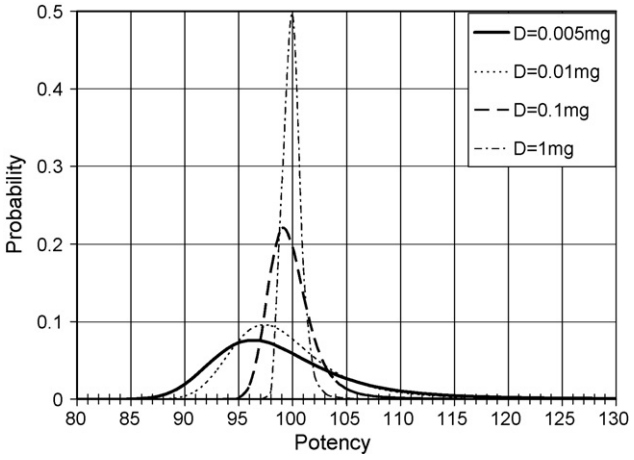


**Fig. 4.** Drug potency distribution at various target dose $D$s. All the curves have the same mean of 100. As $D$ decreases, the span becomes wider and the mode shifts toward under-potency (positive skewness). The shifting is originated from the augment of the number fluctuation for large particles upon the reduction of $D$. The API has a log-normal size distribution with $d_{50}$ = 10 μm and $\sigma_g$ = 3.

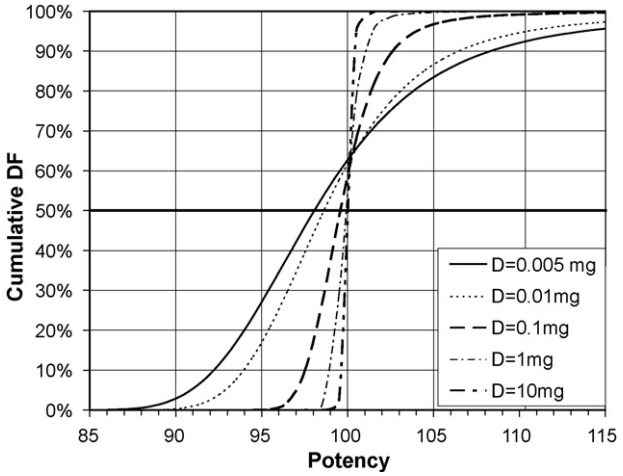


**Fig. 5.** Cumulative potency distribution functions of Fig. 4 reveal that at a low target dose the median (50% line) is less than the average potency of 100. This observation elucidates an important cause, among others, of under-potency which is originated from the positive skewness, independent of the manufacturing process or the ingredients' property.

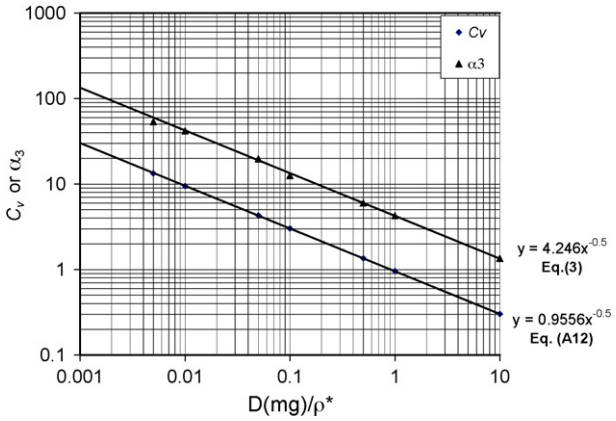


**Fig. 6.** Comparison of $C_v$ and $\alpha_3$ calculated from MC simulation in Fig. 4 (legends) and the predictions (solid curves) calculated from Eq. (3) and Eq. (A12) against the target dose. Note that both $C_v$ and $\alpha_3$ are proportional to $1/\sqrt{D}$.

Here $f(d)$ is the volume fraction for particle size $d$, $\sigma_g$ is the geometric standard deviation; $d_{50}$ is the median diameter. For numerical computations, the truncated lengths are placed at $\pm 4\ln\sigma_g$ about the median.

The probability of passing the USP ⟨905⟩ is simulated by performing content uniformity test a million times; in each time 10 units are constructed to examine the mean and the standard deviation and to obtain *AV* for Stage 1 (Table 1). If it fails, an additional 20 units will be generated for Stage 2. After many repeated sampling, a statistical basis is established and the pass rates for Stages 1 and 2 can be calculated. This computer simulation algorithm is depicted Fig. 2. The program is coded in Fortran and is executed in high-speed workstations. The inputs of the program are the target dose $D$, the true density $\rho$, and the volume fraction-particle size distribution and the outputs are the pass rates of Stages 1 and 2. Note that this numerical simulation can be applied to practically *any* particle size distribution including skewed or multi-modal distributions. It also allows one to implement a cut-off diameter by discarding all the bins that have a particle size larger than the cut-off.

## 3. Results and discussion

To ensure an adequate numerical accuracy within a bearable computation time frame, we have tested several total bins. Fig. 3 depicts the potency distribution using API particles with $d_{50} = 10\,\mu m$, $\sigma_g = 3.5$, and $D/\rho^* = 0.462$ mg under various total bin numbers: $\mathcal{N} = 50, 100, 200, 300$, and 600. A larger $\mathcal{N}$ denotes a finer partition that mimics a continuous distribution on the cost of longer computation time. The figure shows no significant difference after $\mathcal{N}$ is larger than 100, indicative of the independence on the size of the system. An $\mathcal{N} = 300$ is selected for all computations hereafter.

The calculated potency distribution of dosage units and its cumulative distribution are depicted in Figs. 4 and 5. Various target doses ranging from 1 mg to 0.005 mg are simulated from a distribution with $d_{50} = 10\,\mu m$ and $\sigma_g = 3$. This particle size distribution is typically seen from micronized API for low-dose compounds. The curves feature the same mean of 100 but different modes, standard deviations, and skewness. For example, when $D = 1$ mg, the relative standard deviation is 0.951 and the skewness is 3.912. The curve is similar to a normal distribution with the mode close to 100. As the dose decreases, the standard deviation increases, the mode moves towards further left and the skewness becomes larger. A 50% line is constructed in Fig. 5 to elucidate the trend of shifting towards under-potency. As $C_v$ surges upon the decreasing dose, the deviation from normality becomes more severe, indicating a tendency towards an under-potent assay result in finite-number sampling. This tendency, independent of other causes such as loss of drug or analytical error, is originated from the positive skewness. Fig. 6 depicts the comparison of simulated skewness and $C_v$ obtained from Fig. 4 and their analytical counterparts (solid curves) obtained from Eqs. (3) and (A12), which give $\alpha_3 = 4.246(D/\rho^*)^{-0.5}$ and $C_v = 0.9556(D/\rho^*)^{-0.5}$. Here, $\rho^*$ represents the specific (true) density of the API. A strikingly close agreement between the simulation (computer experimentation) and the analytical prediction is observed. This justifies the validity of the MC methodology. In addition, the $-1/2$ slope on the logarithmic plot shown by the simulation data confirms the scaling dependence on $D$ according to Eqs. (1) and (2) and supports the observation of the anomaly in experiment (Fig. 1).

A graphic representation of USP ⟨905⟩ Stage 1 test is depicted in Fig. 7 in which a pyramid area with a flat top (a trapezoid) denotes the pass zone defined by the criteria. Here the $y$-axis denotes the sample standard deviation ($s$) and the $x$-axis denotes the sample potency mean ($\bar{X}$). The flat top is when $\bar{X}$ between 98.5% and 101.5% and $s = 15/2.4 = 6.25$. When $s = 0$, the $\bar{X}$ must fall between 93.5% and 116.5%. Any data falling outside the pass zone indicates a failure to Stage 1. For the batch of dosage units obtained from Fig. 4 with $D = 1$ mg, 10,000 Stage 1 results are shown in Fig. 7(1a). Each dot represents a result obtained from randomly retrieving 10 dosage units from the batch. After each run of the test, the batch is replenished with the same units drawn so that the distribution maintains the same. For comparison, a second batch based on an assumed normal potency distribution of the same $C_v$ is constructed and the same tests are repeated in Fig. 7(1b). It is evident that in Fig. 7(1a) the distribution of data points is highly anisotropic in contrary to the isotropic distribution in Fig. 7(1b). This is a direct consequence from the positive skewness. The comparison also reveals that the pass rate is artificially increased by assuming a normal potency distribution. Such a fallacy becomes increasingly severe for $D = 0.1$ mg as shown in Fig. 7(2a) and (2b). Note for $D = 0.01$ mg the normal distribution assumption renders an underestimate of the pass rate as shown in Fig. 7(3a) and (3b). The comparison confirms significant deviations of the real test results against the Stage 1 criteria from the results based on the normality assumption.

The pass rate of the CU test can be determined by the fraction of the dots falling inside the designated area after a million repetitions. For those failing from Stage 1, Stage 2 is performed. The prediction of how the pass rate changes with the target dose $D$

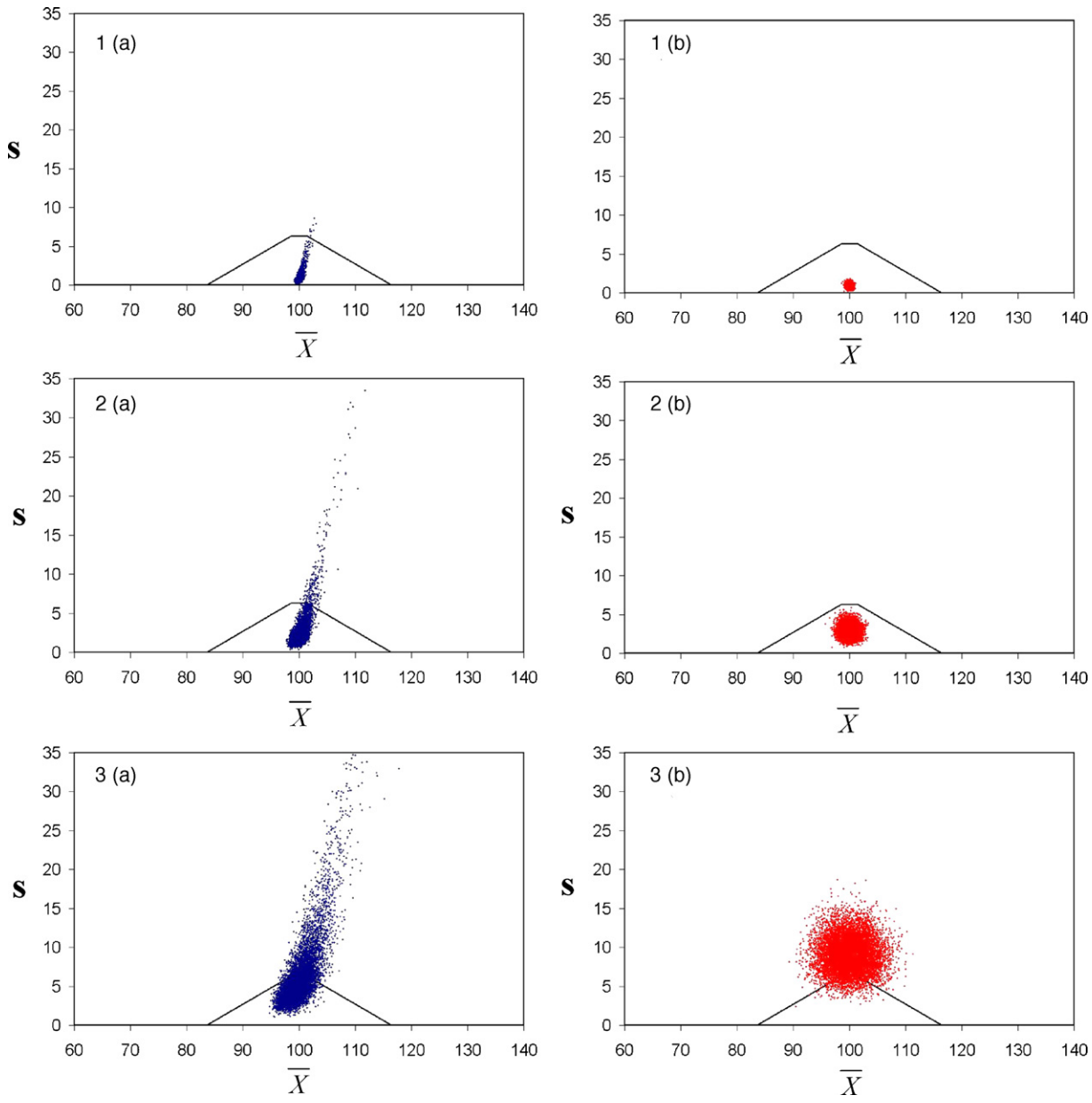


**Fig. 7.** Distribution of the standard deviation ($s$) and the mean $\bar{X}$ of $10^4$ CU tests from Fig. 4. Each dot represents a test result from 10 randomly selected dosage units; the trapezoidal shape is the Stage-1 boundary defined by USP ⟨905⟩. Parts 1a, 2a, and 3a represent $D$ = 1 mg, 0.1 mg, and 0.01 mg, respectively. Parts 1b, 2b, and 3b denote the counterparts simulated under the assumption of a normal potency distribution. It is evident that the skewness renders a higher failure probability at higher $D$ and lower failure probability at lower $D$ than the prediction by an assumed normal distribution.

(mg)/$\rho^*$ is shown in Fig. 8. Here the API has a size distribution of $d_{50}$ = 50 μm and $\sigma_g$ = 2. The solid curve denotes the combined pass rate from Stages 1 and 2. As shown by the curve and the dotted lines, the lowest dose limit for 95% passing rate is 0.16 mg and that for 99% pass rate is 0.3 mg. The long-dashed curve represents the pass rate solely from Stage 1, which is the dominant term when the dose is 0.3 mg or higher. The short-dashed curve denotes the percent contribution from Stage 2 to the combined pass rate. When the dose goes below 0.3 mg, the reliance on Stage 2 becomes significant which is undesirable. For example, in the case of 95% combined pass rate, 23% of the total passing is attributed to Stage 2, whereas only 5% attributed to Stage 2 when the combined pass rate is 99%. As a result, the simulated nomogram is set to a 99% pass rate (Fig. 9). In many applications, the API particle size distributions are within a range of $\sigma_g$ between 2 and 3. A common practice following a three-tier particle size specification of $d_{90}/d_{50}$ = 30/10, 70/25 and 200/75 has been used by the Author's company for nearly 20 years which will be discussed in detail in the forthcoming paper. To further elucidate the underlying reason why API particle size specification is set with $\sigma_g$ < 3, the probability of passing is simulated with a size distribution of $d_{50}$ = 50 μm and $\sigma_g$ = 3 (dot-dashed curve). Evidently the pass rate declines drastically as the size distribution is broaden.

To facilitate the discussion and application of the relations among the median particle size ($d_{50}$), the geometric standard deviation ($\sigma_g$), and the limit of the lowest target dose ($D/\rho^*$), a nomograph based on 99% confidence of passing USP ⟨905⟩ is constructed in Fig. 9. The lines in a descending fashion from the top are corresponding to the following order: $\sigma_g$ = 1.01, 1.5, 2, 2.5, 3, 3.5, and 4, respectively. These lines can be regarded as the maximal $d_{50}$ for a given target dose to warrant a 99% pass rate. For instance, at a given dose of 1 mg, $d_{50}$ has to be less than 20.4 μm if $\sigma_g$ is 3.0 (i.e. $d_{90}$ is less than 83.4 μm as shown in Table 2). Should the API have

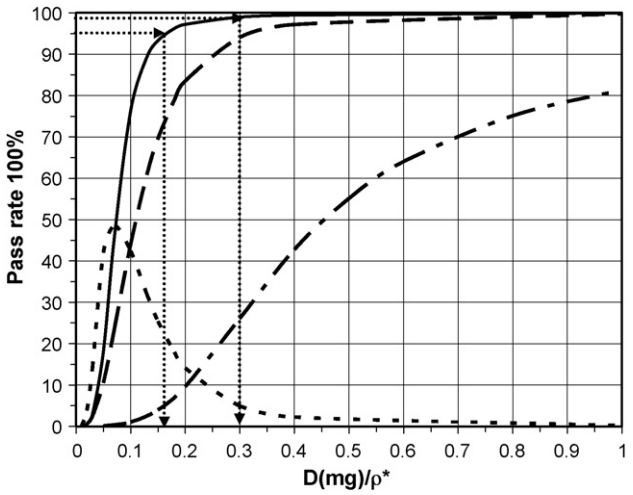


**Fig. 8.** Prediction of the pass rate versus the target dose according to USP ⟨905⟩ CU Criteria. The solid curve denotes the combined pass rate from Stages 1 and 2 for a particle size distribution of $d_{50}$ = 50 μm and $\sigma_g$ = 2. The long-dashed curve denotes the pass rate from Stage 1. The short-dashed curve denotes the fraction of passing from Stage 2. The dot-dashed curve represents the pass rate when the particle size changes to $d_{50}$ = 50 μm and $\sigma_g$ = 3.

**Table 2**
Applications of the nomograph in Fig. 9. Part A depicts the relation between the maximal $d_{90}/d_{50}$ and the lowest dose when $d_{50}$ = 20 μm. Part B depicts the maximal $d_{50}$ when $D/\rho^*$ = 1 mg.

| (A) $d_{50}$ = 20 μm | | |
|---|---|---|
| $\sigma_g$ | $d_{90}/d_{50}$ | $D/\rho^*$ (mg) |
| 1.5 | 1.68 | 0.0027 |
| 2 | 2.43 | 0.022 |
| 2.5 | 3.23 | 0.17 |
| 3 | 4.09 | 0.94 |
| 3.5 | 4.98 | 3.96 |
| (B) $D/\rho^*$ = 1 mg | | |
| $\sigma_g$ | $d_{90}/d_{50}$ | $d_{50}$ (μm) |
| 1.5 | 1.68 | 142.85 |
| 2 | 2.43 | 71.42 |
| 2.5 | 3.23 | 36.16 |
| 3 | 4.09 | 20.41 |
| 3.5 | 4.98 | 12.64 |

a narrower particle size distribution, say, $\sigma_g$ = 2.5, $d_{50}$ can increase up to 36.16 μm. In this way one can set a particle size specification based on the target dose to select an appropriate API processing step according to the capability of the micronizing or milling or sieving equipment. The other way of using the nomograph is to estimate the lowest dose strength that can be made uniformly from a given particle size distribution. For instance, an API with $d_{50}$ at 20 μm and $\sigma_g$ = 2.5, the lowest dose it can be made uniformly is 0.17 mg (Table 2). If the required dose strength is 1 mg, it leaves a comfortable margin for possible non-ideal mixing and analytical error. On the other hand, if $\sigma_g$ = 3, the lowest dose limit is 0.94 mg which may be too close to 1 mg. The API should be further milled or sieved to improve its size distribution. Therefore, the nomograph can be used as an in-process check to determine the acceptability of the API after milling. Lastly, one may use the nomograph to define a design space

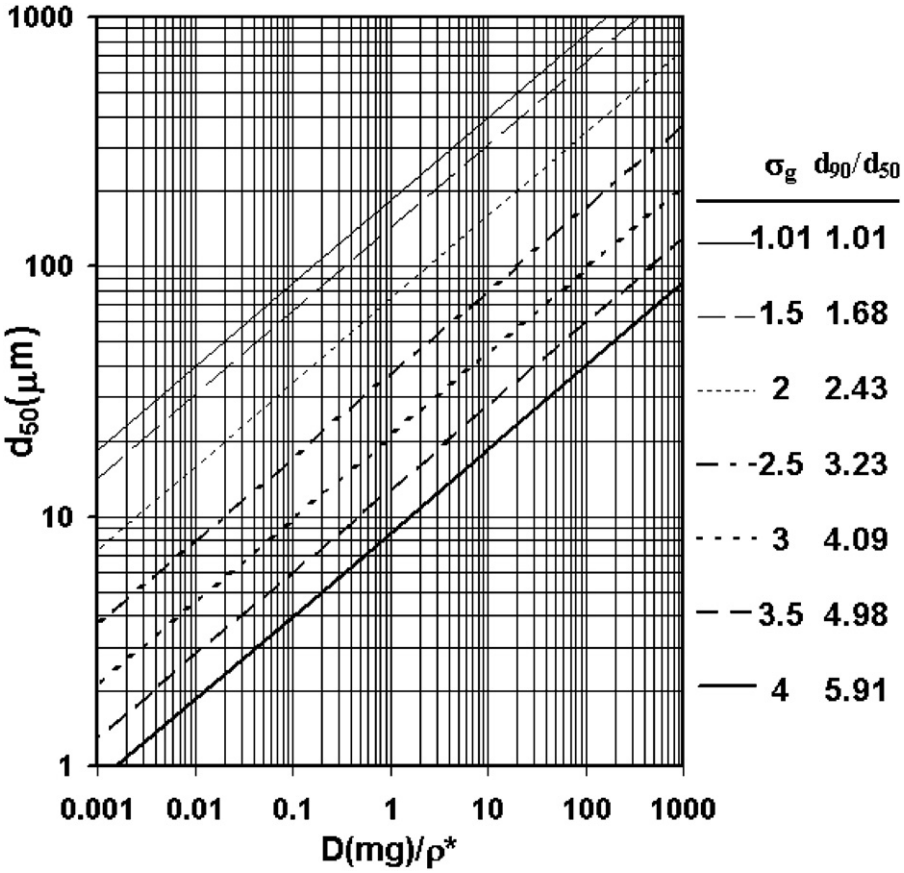


**Fig. 9.** Nomograph of the median particle size ($d_{50}$) versus the dose limit ($D/\rho^*$) at various geometric standard deviations ($\sigma_g$) for 99% combined pass rate of Stages 1 and 2 of USP ⟨905⟩. The drug particle size follows a log-normal distribution. The lines from the top are cases of $\sigma_g$ = 1.01, 1.5, 2, 2.5, 3, 3.5, and 4. The corresponding $d_{90}/d_{50}$ are 1.01, 1.68, 2.43, 3.23, 4.09, 4.98, and 5.91, respectively.

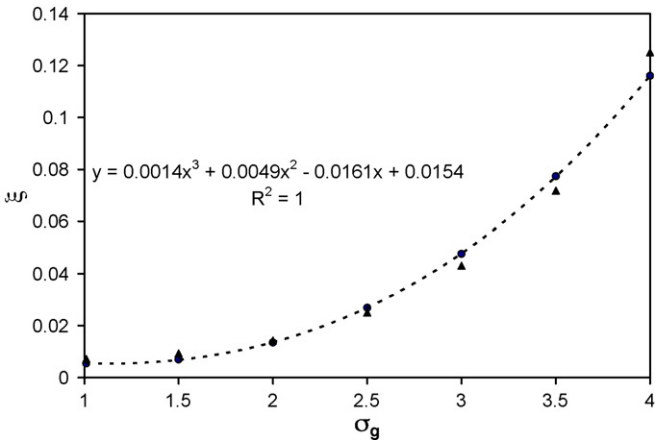


**Fig. 10.** The scaling coefficient $\xi$ (sphere) from Fig. 9 versus $\sigma_g$. The dotted curve exhibits a cubic polynomial fitting. The triangular symbols denote the scaling coefficient obtained from Fig. 3 in the paper by Rohrs et al. for 99% pass rate according to Stage 1 of USP28/NF23.

(FDA, 2003; Yu, 2007; Lionberger et al., 2008) of particle sizes and ensure a certain confidence level in passing the content uniformity test.

As mentioned in Section 2.2, an important feature in Fig. 9 is that all lines of a slope of 1/3 represent the loci of identical potency distribution. The 1/3 power-law relation is universal except when the conformation of particle size distribution changes such as the change of $\sigma_g$ or size cut-off. A power-law equation is, thus, given as

$$d_{50} = \frac{1}{\xi}\left(\frac{D}{\rho^*}\right)^{1/3}, \tag{7}$$

where the scaling coefficient $\xi$ is a function of $\sigma_g$. Fig. 10 depicts the variation of $\xi$ (sphere) against $\sigma_g$. A cubic polynomial (dotted curve) is obtained by data fitting:

$$\xi = 0.0014\sigma_g^3 + 0.0049\sigma_g^2 - 0.0161\sigma_g + 0.0154. \tag{8}$$

Eq. (8) can be used to generate Table 2. The triangular symbols in Fig. 10 denote the scaling coefficient obtained from the nomograph (Fig. 3) given by Rohrs et al. Though the difference is not significant, the interpretation is very different: The nomograph by Rohrs et al. was calculated based on a threshold $C_v$ that assures 99% pass rate of USP28/NF23 Stage 1. In our case, the threshold $C_v$ decreases with $\sigma_g$ and the pass rate is for combined Stages 1 and 2 of USP ⟨905⟩.

Each line in Fig. 9 represents the loci of identical potency distribution with a set of threshold coefficient of variation $C_v^c$ and skewness $\alpha_3^c$ that warrant a 99% pass rate. A list of $\sigma_g$ and the corresponding $C_v^c$ and $\alpha_3^c$ are depicted in Table 3. If $\sigma_g$ is very close to 1, i.e. when the particle size distribution is like a spike, the potency distribution is a normal distribution. Under such a circumstance, $C_v^c$ is 5.724 and the skewness is zero. This threshold can be regarded as the threshold calculated under the assumption of a normal potency distribution. As $\sigma_g$ increases to 3.5, $\alpha_3^c$ increases to 24.648 and $C_v^c$ must decrease to 2.859 to compensate for the skewness. Unfortunately, the new USP ⟨905⟩ criteria did not consider a skewed potency distribution. It improves over the old criteria with graduated smaller $C_v$ when the mean potency is further away from the theoretical 100%. However, the new criteria assume a potency distribution to be normal. When the distribution is skewed with a few large API particles -as most cases would be, the chance of falsely passing the USP criteria increases (Fig. 7). This may post a severe discrepancy when the particle size has a wide distribution or the target dose is very low and results in the release of a sub-quality batch.

**Table 3**
Threshold $C_v^c$ and skewness $\alpha_3^c$ of the potency distribution for 99.0% pass rate as a function of the $\sigma_g$ of the particle size distribution. Note that $C_v^c$ can be significantly lower than the value predicted by an assumed normal potency distribution ($C_v$ = 5.724).

| $\sigma_g$ | $C_v^c$ | Skewness $\alpha_3^c$ |
|---|---|---|
| 1.01 | 5.724 | 0.0585 |
| 1.5 | 5.630 | 0.235 |
| 2 | 4.213 | 1.511 |
| 2.5 | 3.129 | 5.112 |
| 3 | 2.915 | 13.013 |
| 3.5 | 2.859 | 24.648 |

There is, however, an easy remedy to correct a wide API particle size distribution. Since the over-potent skewness is affected mostly by oversized API particles, these particles can be removed by prescreening or milling with an end sieve such as Fritz Mill and Comil. Sieving only works effectively on larger sizes since small particles tend to agglomerate and adhere to the fine sieves, preventing effective removal of the oversized particles. To this account, Monte Carlo simulation is employed with a cut-off particle size representing the sieve opening. The cut-off can be achieved by removing the bins of particle size larger than the cut-off. Fig. 11 is a nomograph of $d_{50}$ versus the lowest dose limit ($D/\rho^*$) with different cut-off particle size for a 99% pass rate. Set A represents $\sigma_g$ = 2 and the cut-off sizes are 300 μm (solid), 500 μm (dashed), and infinite (no cut-off, dotted). As shown in the figure, the lowest dose limit for $d_{50}$ = 100 μm without cut-off is 2.74 mg. It reduces to 0.882 mg for a 500 μm cut-off and to 0.468 mg for a 300 μm cut-off – a five folds reduction in the lowest dose limit. Similarly, Set B represents $\sigma_g$ = 3 and the cut-off sizes are 300 μm (solid), 500 μm (dashed), and infinite (dotted). The lowest dose limit for $d_{50}$ = 100 μm without cut-off is 117.6 mg. It is 1.392 mg for a 500 μm cut-off and 0.486 mg for a 300 μm cut-off – a 240 folds reduction in the lowest dose limit. The non-linearity is originated from the removal of bins from the statistic basis by the cut-off. Since the particle size distributions are truncated at $4\ln\sigma_g$ about the median ($d_{50}$), the largest particle size is $d_{50} \times \sigma_g^4$. When this value is larger than the cut-off ($\lambda_c$), oversized particles are filtered off and the total fluctuation is, thus, suppressed. Consequently, a larger particle size or a smaller target dosage becomes tolerable and the boundary curves bend upwards. The onset $d_{50}$ for such a change is equal to $\lambda_c/\sigma_g^4$ which has the values of 31.25 μm (for $\lambda_c$ = 500) and 18.75 μm (for $\lambda_c$ = 300) μm for set A. For set B, the onsets are 6.172 μm ($\lambda_c$ = 500) and 3.703 μm ($\lambda_c$ = 300), respectively. Though the advantage of removing large particles from an

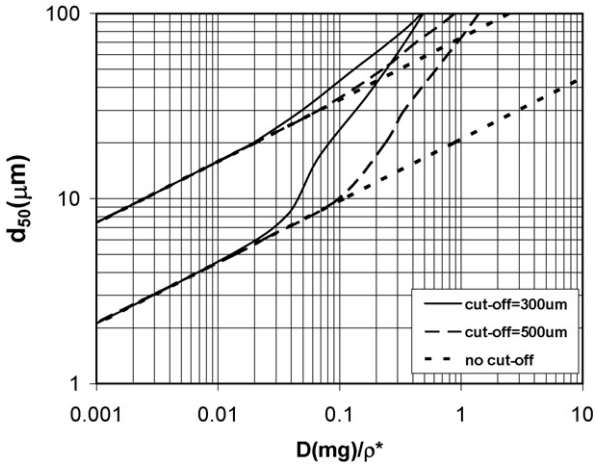


**Fig. 11.** Nomograph of the median particle size ($d_{50}$) versus the dose limit ($D/\rho^*$) with different cut-off size. Set A represents the family of $\sigma_g$ = 2 with a cut-off at 300 μm (solid), 500 μm (dashed), and no cut-off (dotted), respectively. Set B represents the family of $\sigma_g$ = 3 with a cut-off at 300 μm (solid), 500 μm (dashed), and no cut-off (dotted), respectively.

API batch is known to enhance the content uniformity, this study shows for the first time a quantitative comparison on the effectiveness in improving content uniformity brought by a simple sieving step in the manufacture of low-dose drugs.

## 4. Conclusions

Within the frame of random retrieving theory and Poisson distribution, we derived analytically the skewness of the potency distribution and demonstrated that as the target dose decreases, a potency distribution will quickly deviate from normality before $C_v$ becomes significantly large. The positive skewness, originated from the augment of the number fluctuation of large particles, renders a higher probability of obtaining an under-potent CU result, independent of other possible causes.

Monte Carlo simulation was used for the first time to solve the full potency distribution of the random retrieving theory. The simulation results were in agreement with the theoretical analysis and showed a striking anisotropy of data distribution against the prediction based on normality assumption. Consequently, the threshold $C_v^c$ must decrease to compensate for the skewness in order to maintain a certain level of pass rate.

A nomograph for median particle size and dose with a 99% pass rate according to USP ⟨905⟩ criteria was constructed. This nomograph is useful in locating the lowest dose limit for a given particle size distribution or to set particle size specification according to a chosen target dose. The interplays of particle size, standard deviation, and dose render a design space within which a certain confidence level of passing the CU test is ensured.

Lastly, we showed quantitatively that the lowest dose limit can be reduced drastically if a cut-off size is imposed by removing oversized particles. For the distribution $d_{50} = 100\ \mu m$ and $\sigma_g = 3$, the lowest dose limit can be reduced for more than 200 folds if a cut-off length of 300 μm is imposed.

## Acknowledgments

The authors would like to thank Dr. Wendy Dulin for useful discussions. CYH is indebted to Dr. Brian Rohrs for providing the experiment data from his paper.

## Appendix A.

In this appendix, we developed a random retrieving theory similar to the strategy used by Yalkowsky and Bolton (1990). Each dosage unit will randomly draw particles from an ideally mixed blend of excipients and API with a known load and particle size distribution. Though the target dose is low, the number of API particles must be very large in order to warrant a meaningful statistical basis. Assume $n$ is the number of API particles appearing in a dosage unit and $w$ is the mass of a particle. Both $n$ and $w$ are random variables that $n$ follows a Poisson distribution and $w$ follows an equivalent mass distribution converted from the particle size distribution. The potency strength $G$ in a dosage unit is the sum of the mass of $n$ API particles:

$$G = \sum_{i=1}^{n} w_i, \tag{A1}$$

where $w_i$ is the mass of the $i$th particle. Thus, the potency mean and the variance can be expressed as

$$\langle G\rangle \equiv G_o = \langle \sum_{i=1}^{n} w_i\rangle = \langle n\rangle\langle w\rangle \tag{A2}$$

and

$$Var(G) = \langle (G - G_o)^2\rangle = \langle n\rangle Var(w) + Var(n)\langle w\rangle^2. \tag{A3}$$

Here $Var(w)$ and $Var(n)$ represent the variances of $w$ and $n$, respectively. Similarly, the third central moment of $G$ can be expressed as

$$\mu_3(G) = \langle (G - G_o)^3\rangle = \langle n\rangle\mu_3(w) + 3\langle w\rangle Var(w)Var(n) + \langle w\rangle^3\mu_3(n), \tag{A4}$$

where $\mu_3(w)$ and $\mu_3(n)$ are the third central moments of $w$ and $n$, respectively. From the property of a Poisson distribution (Spiegel, 1982), the following identities are found:

$$\langle n\rangle = Var\langle n\rangle = \mu_3(n). \tag{A5}$$

Therefore, Eqs. (A3) and (A4) become

$$Var(G) = \langle n\rangle\langle w^2\rangle \tag{A6-1}$$

and

$$\mu_3(G) = \langle n\rangle\langle w^3\rangle. \tag{A6-2}$$

Following their definitions, the coefficient of variation $C_v$ and the skewness $\alpha_3$ can be expressed in terms of the moments of $w$ and the potency mean:

$$C_v = \frac{Var(G)^{1/2}}{\langle G\rangle} = \frac{\langle w^2\rangle^{1/2}}{\sqrt{\langle n\rangle\langle w\rangle}} = \frac{\langle w^2\rangle^{1/2}}{G_0^{1/2}\langle w\rangle^{1/2}}, \tag{A7}$$

$$\alpha_3 = \frac{\mu_3(G)}{Var(G)^{3/2}} = \frac{\langle w^3\rangle}{\sqrt{\langle n\rangle}\langle w^2\rangle^{3/2}} = \frac{\langle w\rangle^{1/2}\langle w^3\rangle}{G_0^{1/2}\langle w^2\rangle^{3/2}}. \tag{A8}$$

Eqs. (A7) and (A8) are the general forms for *any* particle size distribution. Both equations show an inverse proportionality to the square root of $G_0$ and the de-coupling from particle size distribution (i.e. the moments of $w$). Assume there is no loss of API and the potency mean is 100% of the target dose, i.e. $D = G_0$. We will regard $D$ and $G_0$ interchangeable hereafter. Assuming the mass of each API particle can be expressed as the product of the true density $\rho$ and a volume-equivalent sphere, the moments of $w$ can be expressed in a discrete form:

$$\begin{aligned}\langle w\rangle &= \frac{\pi\rho}{6}\sum_{i=1}^{N} p(d_i){d_i}^3,\\ \langle w^2\rangle &= \left(\frac{\pi\rho}{6}\right)^2\sum_{i=1}^{N} p(d_i){d_i}^6,\\ \langle w^3\rangle &= \left(\frac{\pi\rho}{6}\right)^3\sum_{i=1}^{N} p(d_i){d_i}^9,\end{aligned} \tag{A9}$$

where $p(d_i)$ is the number frequency for particles with a diameter $d_i$. The volume fraction $f_i$ for API particles with a diameter $d_i$ can be expressed as

$$f_i = \frac{p(d_i){d_i}^3}{\sum_{j=1}^{N} p(d_j){d_j}^3}, \tag{A10}$$

where $N$ denotes the total number of the particle sizes.

Thus, Eq. (A8) and (A7) can be written as

$$\alpha_3 = \left(\frac{\pi\rho}{6D}\right)^{1/2}\frac{\sum_{i=1}^{N} f_i d_i^6}{\left(\sum_{i=1}^{N} f_i d_i^3\right)^{3/2}}, \tag{A11}$$

$$C_v = \sqrt{\frac{\pi\rho}{6D}}\sqrt{\sum_{i=1}^{N} f_i {d_i}^3}. \tag{A12}$$

Note that Eq. (A12) was first given by Johnson (1972).

For the special case of a log-normal particle size distribution, the frequency density function is written as

$$\tilde{p}(d) = \frac{1}{\sqrt{2\pi}\eta d} e^{-1/2((\ln d - \lambda)/(\eta))^2}, \tag{A13}$$

where $\eta = \ln \sigma_g$ and $\lambda = \ln d_{50}$. The $k$th raw moment of the log-normal distribution are (Aitchison and Brown, 1957)

$$\begin{aligned} \mu_1' &= \langle d \rangle = d_m = e^{\lambda + \eta^2/2} = e^{\lambda}(1 + c^2)^{1/2}, \\ \mu_k' &= \langle d^k \rangle = \mu'^k_1 (1 + c^2)^{k(k-1)/2}, \end{aligned} \tag{A14}$$

where $c$ is the arithmetic coefficient of variation and $d_m$ is the arithmetic mean diameter of the particle size. Thus, Eq. (A9) can be readily converted to

$$\begin{aligned} \langle w \rangle &= \frac{\pi\rho}{6}\mu_3', \\ \langle w^2 \rangle &= \left(\frac{\pi\rho}{6}\right)^2 \mu_6', \\ \langle w^3 \rangle &= \left(\frac{\pi\rho}{6}\right)^3 \mu_9'. \end{aligned} \tag{A15}$$

Substituting Eq. (A15) into Eq. (A8), the skewness becomes

$$\alpha_3 = \sqrt{\frac{\pi\rho}{6D}} d_m^{3/2} (1 + C^2)^{15}. \tag{A16}$$

Similarly, one can easily recover the equation given by Yalkowsky and Bolton (1990) by substituting Eq. (A15) into Eq. (A7):

$$C_v = \sqrt{\frac{\pi\rho}{6D}} d_m^{3/2} (1 + c^2)^6. \tag{A17}$$

## References


Aitchison, J., Brown, J.A.C., 1957. The Lognormal Distribution. Cambridge University Press.

Armitage, P., Berry, G., Matthews, J.N.S., 2001. Statistical Methods in Medical Research. Wiley-Blackwell, pp. 292–297.

Bergum, J.S., Li, H., 2007. Acceptance limits for the new ICH USP 29 content-uniformity test. Pharm. Tech., 90–100.

Bonate, P.L., 2001. A brief introduction to Monte Carlo simulation. Clin. Pharmacokinet. 40, 15–22.

Buckton, G., 1995. Interfacial Phenomena in Drug Delivery and Targeting. Hardwood Academic Publishers, Switzerland.

Byron, P.R., Peart, J., Staniforth, J.N., 1997. Aerosol electrostatics. I. Properties of find powder before and after aerosolization by dry powder inhalers. Pharm. Res. 14, 697–705.

Cartilier, L.H., Moes, A.J., 1989. Effect of drug agglomerates upon the kinetics of mixing of low dosage cohesive powder mixtures. Drug Dev. Ind. Pharm. 15, 1911.

Cholayudth, P., 2008. Using Bergum's new method and MS excel to determine the probability of passing the new ICH USP 29 content uniformity test. J. Valid. Tech. Winter, 62–71.

Egermann, H., Kemptner, I., Pichler, E., 1985. Effects of interparticulate interactions on mixing homogeneity. Drug Dev. Ind. Pharm. 11, 663–676.

European Pharmacopoeia, 2008. 2.9.40. Uniformity of Dosage Units, pp. 3325–3327.

Food and Drug Administration, 2003. Final report on pharmaceutical cGMPs for 21st century—a risk-based approach.

Gordon, R.E., Rosanske, T.W., Fonner, D.E., Anderson, N.R., Banker, G.S., 1990. Granulation technology and tablet characterization. In: Lieberman, H.A., Lachman, L., Schwartz, J.B. (Eds.), Pharmaceutical Dosage Forms, Tablets vol. 2. Marcel Dekker Inc., New York.

Hersey, J.A., 1967. Assessment of homogeneity of powder mixtures. J. Pharm. Pharmac. 19, 168–176.

Huang, C.Y., Muthukumar, M.M., 1997. Effects of shear on order–disorder and order–order transitions in block copolymers. J. Chem. Phys. 107, 5561–5571.

Israelachvili, J., 1995. Intermolecular & Surface Forces, 5th ed. Academic Press Ltd.

Johnson, K.C., 2009. Particle size of drug substance and product content uniformity—theoretical considerations. In: Zheng, J. (Ed.), Formulation and Analytical Development for Low-Dose Oral Drug Products. Wiley, NJ (Chapter 3).

Johnson, M.C.R., 1972. Particle size distribution of the active ingredient for solid dosage forms of low dosage. Pharm. Acta Helv. 47, 546–559.

Johnson, M.C.R., 1974. Particle-size requirements related to content uniformity of solid dosage forms. J. Pharm. Sci. 63, 1961–1963.

Johnson, M.C.R., 1975. The effect of particle size upon mixture homogeneity. Pharm. Acta Helv. 50, 60–63.

Jullien, R., Meakin, P., 1990. A mechanism for particle size segregation in three dimensions. Nature 344, 425–427.

Lacey, P.M.C., 1943. Mixing of solid particles. Trans. Inst. Chem. Eng. 21, 53–59.

Lachiver, E.D.R., Abatzoglou, N., Cartilier, L., Simard, J.S., 2006. Insights into the role of electrostatic force on the behavior of dry pharmaceutical particulate systems. Pharm. Res. 23, 997–1007.

Lionberger, R.A., Lee, S.L., Lee, L.M., Raw, A., Yu, L.X., 2008. Quality by design: concepts for ANDAs. AAPS J. 10, 268–276.

Mamaluy, M., Huang, C.Y., 2004. Effect of external Gaussian field on phonon spectrum of linear atomic chains. Physica E 22, 912.

Orr, N.A., Sallam, E.A., 1978. Content uniformity of potent drug in tablets. J. Pharm. Pharmac. 30, 741–747.

Orr, N.A., Shotton, E., 1973. The mixing of cohesive powders. Chem. Eng. 269, 12–18.

Press, W.H., Teukolsky, S.A., Vetterling, T., Flannery, B.P., 2007. Numerical Recipes. Cambridge University Press.

Poole, K.R., Taylor, R.F., Wall, G.P., 1964. Mixing powders to fine-scale homogeneity: studies of batch mixing. Trans. Inst. Chem. Eng. 24, 305–315.

Podczeck, F., 1998. Particle–Particle Adhesion in Pharmaceutical Powder Handling. Imperial College Press.

Rhodes, M., 2008. Introduction to Powder Technology. John Wiley & Sons Ltd.

Rohrs, B.R., Amidon, G.E., Meury, R.H., Secreast, P.J., King, H.M., Skoug, C.J., 2006. Particle size limits to meet USP content uniformity criteria for tablets and capsules. J. Pharm. Sci. 95, 1049–1059.

Rubinstein, R.Y., Kroese, D.P., 2008. Simulation and the Monte Carlo Method. John Wiley & Son, NJ.

Sallam, E., Orr, N.A., 1985. Content uniformity of ethinyloestradiol tablets 10 μg: effect of variations in processing on the homogeneity after dry mixing and after tableting. Drug Dev. Ind. Pharm. 11, 607–633.

Sallam, E., Orr, N.A., 1986. Studies relating to the content uniformity of ethinyloestradiol tablets 10 μg: effect of particle size of ethinyloestradiol. Drug Dev. Ind. Pharm. 12, 2015–2042.

Spiegel, M.R., 1982. Theory and Problems of Probability and Statistics. McGraw-Hill Inc, pp. 111–112.

Stange, K., 1954. Die Mischgute einer Zufallsmischung als Grundlage zur Beurteilung von Mischversuchen. Chemie Ingenieur Technik 26, 331–337.

Train, D., 1960. Pharmaceutical aspects of mixing solids. Pharm. J. 185, 129–134.

USP31-NF29, 2009. General Chapters: ⟨905⟩ Uniformity of Dosage Units, p. 363.

Yalkowsky, S.H., Bolton, S., 1990. Particle size and content uniformity. Pharm. Res. 7, 962–966.

Yu, L.X., 2007. Pharmaceutical quality by design: product and process development, understanding, and control. Pharm. Res. 25, 781–791.

Zhang, Y., Johnson, K.C., 1997. Effect of drug particle size on content uniformity of low-dose solid dosage forms. Int. J. Pharm. 154, 179–183.

Zheng, J. (Ed.), 2009. Formulation and Analytical Development for Low-Dose Oral Drug Products. Wiley, NJ.